Structure and Stability of a Model Pyrimidine−Purine−Purine DNA Triple Helix with a GC·T Mismatch by Simulation†

Samantha Weerasinghe, Paul E. Smith, and B. Montgomery Pettitt*

Department of Chemistry, University of Houston, Houston, Texas 77204-5641

Received July 17, 1995; Revised Manuscript Received September 29, 1995®

ABSTRACT: A 1.5 ns long molecular dynamics simulation was conducted to compare the structure and stability of a model DNA triplex in saline solution with that found from experiments. The model DNA was an antiparallel py·pu·pu (CG·G) 7-mer structure which contained a GC·T mismatch triplet at the middle of the sequence. The local conformation of the mismatch triplet and the effects of this triplet on the global helical structure suggest that the GC·T triplet forms stable hydrogen bonds and shows distortions from an in-plane alignment. The overall rms deviation of the triplex is similar to one without a mismatch, although the thymine base in the mismatch triplet shows significantly higher mobility. A high coordination probability for water between the G and T bases in the mismatch triplet was observed to have an effect on the stability of non-hydrogen-bonded base pairs. Average helical parameters, sugar pucker, and backbone dihedral angles indicate that the CG·G triplets on the 3′ side of the mismatch triplet possess different structural and dynamical properties than that of the 5′ side. These observations are consistent with recently available experimental results and provide an interpretation of the observed experimental structure. They also suggest that inclusion of explicit water molecules is necessary in order to understand and predict the interaction between the third strand and duplex DNA.

There has been significant progress in both experimental (Greenberg & Dervan, 1995; Radhakrishnan & Patel, 1993; Beal & Dervan, 1991; Durland et al., 1991; Moser & Dervan, 1987; Rajagopal & Feigon, 1989) and theoretical (Weerasinghe et al., 1995; Piriou et al., 1994; Cheng & Pettitt, 1992a; Laughton & Neidle, 1992) studies toward the understanding of the structure, stability, and thermodynamics of triplex formation. Findings from these studies have given insight into the possible applications in sequencing and the control of gene expression through binding of a third strand to duplex DNA (Sun & Hélène, 1993; Wilson et al., 1993; Hélène & Toulme, 1990; Letai et al., 1988). Most of the theoretical studies have focused on the binding of a third strand to a homopolymer purine−pyrimidine (pu·py) duplex (Cheng & Pettitt, 1992b). These early assessments were important in the understanding of the nature of binding of a third strand to a duplex sequence. In order to further our knowledge of the formation of triplexes, one has to understand the factors behind the stability of different triplexes especially with nonhomo-pu·py duplexes in solution.

The molecular dynamics (MD) simulation method has been used successfully in studies of a variety of biological systems, including proteins (McCammon & Harvey, 1987), duplex DNA (Swaminathan et al., 1991; Forester & McDonald, 1991), and triplex DNA (Mohan et al., 1993b; Weerasinghe et al., 1995) in aqueous solutions. In principle, comparison of the simulation with experiments should be able to provide evidence regarding the quality of the initial structure of the triplex and the force field/protocol, as well as a structural and dynamical description of the behavior of the triplex DNA in salt solutions. A previous simulation of a homopolymer, $(CG·G)_7$, triplex DNA (Weerasinghe et al., 1995) provided structural information concerning the proximal water and salt which was recently shown to be consistent with the interpretation of vibrational spectroscopy (White & Powell, 1995).

A reasonable initial structure for a triplex is required for a successful MD simulation to investigate the structural and dynamical factors for the stability of a DNA triplex in a salt solution. The partial low-resolution structures of several triple helices have been determined by X-ray fiber diffraction (Arnott & Selsing, 1974; Arnott et al., 1976; Piriou et al., 1994), and segments of triple helices have been observed in tRNA X-ray crystal structures at higher resolution (Kim et al., 1974; Robertus et al., 1974). With such limited data, some modeling is required to produce consistent atomic coordinates for a triplex, such as that required for a MD simulation. In the present study, we have employed a structure consisting of seven base planes arranged as determined by a previous model-built triplex (Cheng & Pettitt, 1992b). Several recent MD refined NMR structures appeared after the current simulation had commenced (Radhakrishnan & Patel, 1993; Dittrich et al., 1994). This allows us the opportunity to validate the information from this and other simulations with similar protocols as well as affording an interpretation of the various experiments (Singleton & Dervan, 1994; Radhakrishnan & Patel, 1993; Dittrich et al., 1994; J. Ji and X. Gao, unpublished results).

Several recent experimental studies have been conducted on triplex DNA that contain a GC·T mismatch with parallel orientation (Radhakrishnan & Patel, 1993; Mergny et al., 1991) and with antiparallel orientation (Dittrich et al., 1994; Griffin & Dervan, 1989; Beal & Dervan, 1992) of the third strand, which suggest that the structure is reasonably stable in aqueous solution. Of the common bases, T in the third strand is the least destabilizing base when there is a G·C

† This work was partially supported by the Texas Coordinating Board, the Robert A. Welch Foundation, the NIH, and the National Science Foundation. SDSC is thanked for generous computational support.

® Abstract published in *Advance ACS Abstracts,* November 15, 1995.

0006-2960/95/0434-16269$09.00/0

reversal in the duplex (Griffin & Dervan, 1989; Mergny et al., 1991; Beal & Dervan, 1992; Greenberg & Dervan, 1995). Therefore, with the aim of better understanding the structural and dynamical effects of this mismatch on the stability of the triplex and its environment, we have performed a 1.5 ns long molecular dynamics trajectory. We have used the following notation and labeling to describe the strands and the different triplet planes of the triplex DNA throughout this paper.

3′	5′	3′	
C_1	G_{14}	G_{15}	plane 1
C_2	G_{13}	G_{16}	plane 2
C_3	G_{12}	G_{17}	plane 3
G_4	C_{11}	T_{18}	plane 4
C_5	G_{10}	G_{19}	plane 5
C_6	G_9	G_{20}	plane 6
C_7	G_8	G_{21}	plane 7
I	II	III	

Bases denoted by G_4, C_{11}, and T_{18} represent the mismatch triplet in the triplex DNA. The simulation was performed with explicit solvent and counterions. We anticipate that solvation, screening, and specific cation coordination are important in differentiating the stabilities of various possible conformations. Furthermore, we are able to follow the simulated dynamics of the furanose pucker and backbone conformation, which are of recent experimental interest (Wilson et al., 1993; Letai et al., 1988; Ouali et al., 1993).

The study presented in this paper is arranged as follows. In Methods we present the model and method of simulation along with a description of the triplex DNA model and the solvent environment. We give the results and discussion of the current study in Results. The first part of the Results section describes the structure and the energetics of the model DNA; the latter part describes the behavior of the solvent and ions around the triplex model. In the Discussion section a general discussion of the present work is presented. Conclusions are given in the Discussion.

METHODS

The building of the initial structure has been discussed in detail earlier (Vlijmen et al., 1990; Cheng & Pettitt, 1992a). The first and second strands form a Watson–Crick duplex DNA (Watson & Crick, 1953). The bound third strand has an antiparallel orientation with respect to the second strand and reverse-Hoogsteen base pairing. The initial model structure was built with a helical rise of 3.04 Å and a helical twist of 32.7° and with initial sugar puckers of furanose in the A-form. These initial parameters are the same as the control simulation on a $(CG{\cdot}G)_7$ model triplex (Weerasinghe et al., 1995). The model structure was placed in a cubical box (L = 32.0 Å) with the helical axis parallel to the z-direction. We found 890 water molecules were needed to attain approximately 1 g/mL water density in the simulation box. To maintain electroneutrality of the system, 21 Na^+ ions were added by randomly replacing water molecules. Another 32 individual ions, 16 Na^+ and 16 Cl^-, were added, by random water replacement, to bring the system to approximately 1 M salt concentration. The model system consisted of 837 water molecules, 37 Na^+ ions, and 16 Cl^- ions along with the model triplex DNA and thus should be quite close in thermodynamic state to the simulation of the homopolymer reported previously (Mohan et al., 1993; Weerasinghe et al., 1995).

The same force field and the simulation protocol as in the previous study (Weerasinghe et al., 1995) were used here. Briefly, for triplex DNA, we employed the all-atom force field in CHARMM22 release (Brooks et al., 1983); for water the enhanced simple point charge (SPC/E) model (Berendsen et al., 1987) was used, and for Na^+ and Cl^- ions potential parameters from Chandrasekhar et al. (1984) were used. The simulation was performed in the microcanonical ensemble or constant number, N, volume, V, and energy, E. Velocities were initially assigned from a Maxwell–Boltzmann distribution at an initial temperature of 300 K. All electrostatic interactions were calculated using the Ewald summation method (Ewald, 1921; de Leeuw et al., 1980). To integrate the equations of motion, the velocity version of the Verlet algorithm (Allen & Tildesley, 1987; Swope et al., 1982) was used with a 2 fs time step and with SHAKE bond constraints modified for the velocity Verlet integrator (Ryckaert et al., 1977).

As indicated earlier, the same minimization and equilibration scheme used in the previous simulation (Weerasinghe et al., 1995) was utilized here. Before the trajectory was begun, ten steps of steepest descent minimization was used to remove any large strain in the initial model. During the first 60 ps of the trajectory the DNA was kept rigid while the solvent and counterions diffused around the triplex, under the influence of the force field. Previous simulations have demonstrated that the main features of the ionic atmosphere are well established during this time period (Mohan et al., 1993b), when Ewald electrostatics as opposed to truncation are used (Smith & Pettitt, 1991). After the equilibration period, the solvent molecules and ions were fixed at their respective positions and the DNA was allowed to relax for 1 ps. The DNA was then kept rigid, and solvent molecules and ions were allowed to move for another picosecond. We continued this process by alternatively clamping and unclamping the DNA, for total of a 25 ps, increasing the length of the simulation time of the alternative segments toward the end. Subsequently, all the particles were then allowed to move for 5 ps during which time the velocities were scaled to maintain a temperature near 300 K. The simulation was continued for another 10 ps without any constraints or velocity scaling, after which we observed that the total energy was constant, and the temperature and pressure of the system were stable (a total of 100 ps). We then started a 1.4 ns long trajectory of the heteropolymer triple-helical DNA in salt–water solution. Configurations and velocities were saved at 0.1 ps intervals for analysis.

For subsequent analysis, the global helical axis of the short triplex was assigned by calculating the moment of inertia tensor of the triplex and diagonalizing for each configuration. The directional vector of the smallest principle moment of inertia was taken as the instantaneous global helical axis. We chose the direction of the 3′ end of strand I as the positive direction of the global helical axis for our analysis.

The formulas for triplex helical parameters given in Appendix B in the previous paper (Weerasinghe et al., 1995) can be expressed in more general form (using the same notations therein) as follows: rise, $(\mathbf{r}_{ij}{\cdot}\mathbf{c}_i)$; slide, $(\mathbf{r}_{ij}{\cdot}\mathbf{b}_i)$; shift, $(\mathbf{r}_{ij}{\cdot}\mathbf{a}_i)$; twist, $\cos^{-1}[\mathbf{a}_i(\mathbf{b}_j{\cdot}\mathbf{c}_i)/|\mathbf{b}_j{\cdot}\mathbf{c}_i|]$; roll, $(\pi/2) - \cos^{-1}(\mathbf{b}_j{\cdot}\mathbf{c}_i)$; and tilt, $(\pi/2) - \cos^{-1}(-\mathbf{a}_j{\cdot}\mathbf{c}_i)$; where $\mathbf{r}_{ij}$ is the vector between the center of masses of two adjacent base triplet planes, i

Table 1: Root Mean Square Deviation from the Initial Structure for Selected Groups of Atoms in the Triplex

group	rms deviation mismatch[a] (Å)	rms deviation homo[b] (Å)
strand I	2.09 ± 0.25	1.88 ± 0.36
strand II	1.08 ± 0.11	1.45 ± 0.11
strand III	2.13 ± 0.18	2.24 ± 0.52
base	1.50 ± 0.15	1.23 ± 0.21
sugar	1.93 ± 0.17	1.95 ± 0.39
phosphate	2.24 ± 0.17	2.90 ± 0.44
all	1.83 ± 0.15	1.89 ± 0.33

[a] This work. [b] Weerasinghe et al., 1995.

and j, and $\mathbf{a}_i$, $\mathbf{b}_i$, and $\mathbf{c}_i$ are the unit vectors of the ith base triplet plane.

Coulomb interaction energies calculated in both r-space and k- (*or* reciprocal) space were not deconvoluted into their respective chemical components, due to the high computational demand of the k-space energy. Therefore, only r-space energy components within the traditional spherical region are reported in the Results section.

RESULTS

(A) Triplex Structure and Dynamics. The first 100 ps of the trajectory was used for the equilibration of the triplex in the saline solution as described in the previous section. Stability of the triplex was studied by following the rms deviation of the structure from the initial model. A summary of the rms deviation of different components of the triplex is given in Table 1. Comparable deviations obtained from the MD simulation of the homopolymer d(CG•G)$_7$ (Weerasinghe et al., 1995) are also given in Table 1. Both terminal base triplet planes were neglected from the rms calculation to eliminate end effects. As seen in the simulation of d(CG•G)$_7$, base units in the triplex show the least rms deviation whereas phosphate groups give the largest rms deviation. The third strand shows the largest deviation compared to the first and second strands. Calculated rms deviations of different components of the mismatch triplex and the homopolymer triplex display the same basic trends. Laughton et al. have reported a lower than 2.0 Å rms deviation of the time-average MD structure of a low-pH DNA triple helix, d(TC)$_5$d(GA)$_5$d(C$^+$T)$_5$, from their initial model over a short simulation of 30 ps (Laughton & Neidle, 1992). The current simulation stayed beneath 1 Å rms deviation after being clamped for a comparable length of time.

To more closely examine the effects of the mismatch triplet on the stability of the triplex, rms deviations of individual bases, phosphate groups, and furanose rings were also calculated. These results are given in Table 2. The thymine base, along with the accompanying phosphate group and sugar ring, shows a higher rms deviation than other base phosphate groups and furanose rings. The average rms deviation of the thymine base is larger than the other bases. The overall rms deviation and radius of gyration of the triplex are presented in Figure 1. Most of the deviations from the model-built structure occurred during the 50 ps long equilibration period, as seen in Figure 1a, while the next 700 ps of the production run showed a slow increase in rms deviation of the triplex. In the last 700 ps of the trajectory the triplex stayed in an apparently equilibrium state with an

Table 2: Root Mean Square Deviations (and Their Fluctuations) for Bases, Phosphate Groups, and Furanose Rings in the Triplex[a]

	base (Å)	phosphate (Å)	sugar (Å)
C_2	1.79(0.43)	2.81(0.70)	2.40(0.56)
C_3	2.17(0.32)	2.96(0.48)	2.67(0.37)
G_4	1.70(0.27)	2.86(0.42)	2.51(0.37)
C_5	1.21(0.22)	2.33(0.42)	1.61(0.41)
C_6	1.02(0.20)	1.65(0.36)	1.11(0.25)
G_9	0.86(0.26)	1.24(0.27)	1.11(0.25)
G_{10}	0.66(0.18)	0.75(0.22)	0.80(0.34)
C_{11}	1.16(0.24)	0.89(0.23)	0.89(0.23)
G_{12}	1.30(0.21)	0.98(0.23)	0.91(0.24)
G_{13}	1.39(0.25)	1.20(0.18)	1.21(0.25)
G_{16}	0.95(0.19)	1.79(0.31)	1.21(0.25)
G_{17}	1.61(0.31)	2.17(0.34)	2.13(0.29)
T_{18}	2.59(0.53)	3.78(0.73)	2.34(0.37)
G_{19}	0.89(0.29)	1.46(0.50)	1.34(0.44)
G_{20}	1.90(0.25)	3.19(0.46)	3.66(0.51)

[a] For this calculation, at each time step, entire triplex DNA was least-squares-fit to the initial structure, and then the rms deviations of separate parts were evaluated.

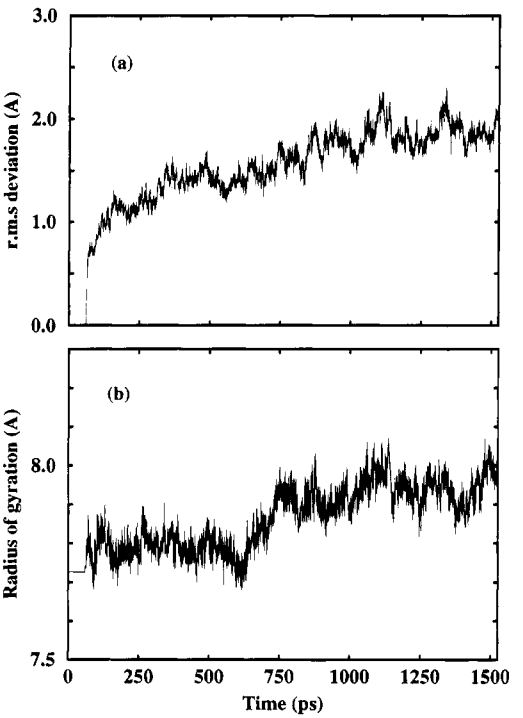

FIGURE 1: Plot of the (a) total rms deviation and (b) radius of gyration (Å) of triplex DNA as a function of simulation time.

average rms deviation of 1.83 ± 0.15 Å. Figure 1b shows the radius of gyration of the triplex (note that we have omitted the first and the seventh base triplet planes from the calculation of the radius of gyration). The figure indicates that the radius of gyration of the triplex also converges during the last 700 ps of the trajectory, confirming the structural stability of the triplex in saline solution. The rms deviation and the radius of gyration of the (CG•G)$_7$ triplex (Weerasinghe et al., 1995) also showed the same trend.

Even though the common helical parameters were initially developed for duplex DNA, extension of these definitions to triplex DNA has been proposed (Weerasinghe et al., 1995). The triplex DNA helical parameters give a measure of the structure and stability of the DNA in salt−water solution. Only the helical parameters with respect to adjacent base triplet planes, namely, rise, shift, slide, twist, roll, and tilt, were considered. Figure 2 gives the average three transla-

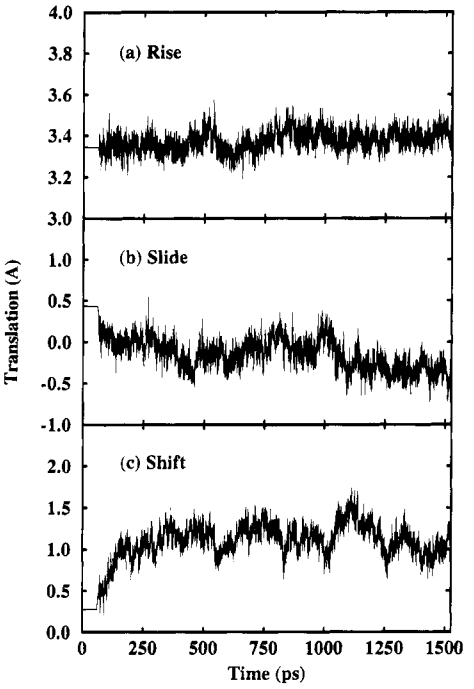

FIGURE 2: Plot of the average (a) helical rise, (b) slide, and (c) shift (in angstroms) between two adjacent base triplet planes as a function of the simulation time.

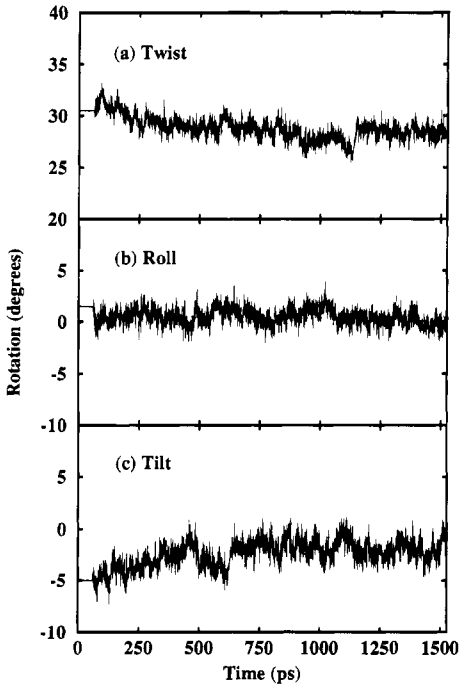

FIGURE 3: Plot of the average (a) twist, (b) roll, and (c) tilt (in degrees) of two adjacent base triplet planes as a function of simulation time.

tional parameters, rise, slide, and shift, and Figure 3 presents the three average rotational parameters, twist, roll, and tilt, as a function of the simulation time. The initial rise and twist are slightly different from those of the model structure. This discrepancy is due to the steepest descent minimization of the structure before the start of the trajectory. The terminal base triplet planes were excluded from the calculation of average parameters. While the rise was quite stable, the slide and the shift were relaxed from the model structure by 0.5 and 1.0 Å, respectively, during the first 400 ps. A sudden increase of the average twist starting around 1300 ps was

Table 3: Average Helical Parameters (and Fluctuations) of Different Pairs of Base Triplet Planes

	base triplet planes			
parameter	2 and 3	3 and 4	4 and 5	5 and 6
rise (Å)	3.24(0.12)	2.26(0.10)	3.50(0.12)	3.59(0.11)
slide (Å)	0.81(0.26)	−0.51(0.34)	−0.54(0.57)	−0.65(0.32)
shift (Å)	0.52(0.24)	1.12(0.35)	1.25(0.41)	1.62(0.31)
twist (deg)	41.78(2.96)	37.40(6.75)	14.91(5.01)	18.69(2.92)
roll (deg)	3.44(2.03)	2.82(1.68)	−1.41(1.79)	−3.04(1.47)
tilt (deg)	−8.05(2.31)	−5.26(2.68)	1.82(2.30)	4.05(2.65)

Table 4: Average Hydrogen Bond Distances by Atom Type for the Last 800 ps of the Trajectory

hydrogen bond	heavy atom distance (Å)
$G_{II}N2 \cdot C_IO2$	2.96 ± 0.17
$G_{II}N1 \cdot C_IN3$	3.02 ± 0.11
$C_IN4 \cdot G_{II}O6$	2.98 ± 0.17
$G_{III}N2 \cdot G_{II}O6$	2.88 ± 0.15
$G_{III}N1 \cdot G_{II}N7$	3.14 ± 0.18
$C_{II}N4 \cdot T_{III}O4$	2.87 ± 0.15

mainly due to the movement of the thymine base and was correlated with a change of the δ dihedral angle of the backbone phosphate group. The average shift and the average tilt are also correlated with this change of twist angle. Since the average rise does not show a noticeable change at this time, this motion appears to be an in-plane movement of the thymine base. Even with this fluctuation of the mismatched thymine base, the overall apparent stability of the triplex was not disturbed. Although the average helical parameters indicate the overall stability of the triplex in the saline solution, the effects of the presence of the GCT mismatch on the triplex structure may be more localized. Therefore, the average helical parameters for adjacent pairs of base triplet planes were calculated and are given in Table 3. The results in Table 3 indicate that the structure of the triplex on one side of plane 4 (mismatch plane) is different from that on the other side. The average rise between pairs of planes 2−3 and 3−4 is lower than the average rise between pairs of planes 4−5 and 5−6. This difference is observed in many of the other relative helical parameters except for slide and shift (see Table 3). The lower part of the triplex (planes 2 and 3) shows a larger twist and a somewhat smaller average rise while the top part (planes 5 and 6) shows a higher rise and smaller average twist. Radhakrishnan and Patel (1993) have recently reported that the 5′-d(TpG)-3′ base steps in their refined structures showed an increase in helical rise and decrease in helical twist, while the reverse was observed at 5′-d(GpT)-3′ steps. The average helical parameters presented in Table 3 are in qualitative agreement with the above experimental findings.

Hydrogen bonds are important for the interbase stability and sequence recognition of the triplex. Between bases in a CG·G base triplet plane, there are five possible hydrogen bonds, namely, GN2·CO2, GN1·CN3, and CN4·GO6 between the Watson−Crick pairs in strands I and II and GN2·GO6 and GN1·GN7 between the bases in strands II and III. In plane 4 there are four possible hydrogen bonds, three bonds between the Watson−Crick base pair and one possible hydrogen bond between the C_{11} and T_{18} bases, CN4·TO4. The average hydrogen bond distances over the last 800 ps of the trajectory are given in Table 4. These average values indicate stable hydrogen bonds between bases with small

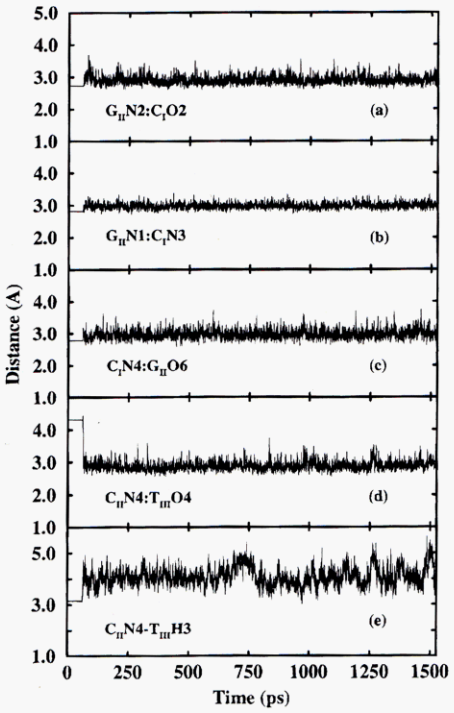

FIGURE 4: Plot of the hydrogen bonds between the central (a−c) Watson−Crick base pair and (d) Hoogsteen pair and (e) the distance between $C_{11}N_4$ and $T_{18}H3$ as a function of the simulation time.

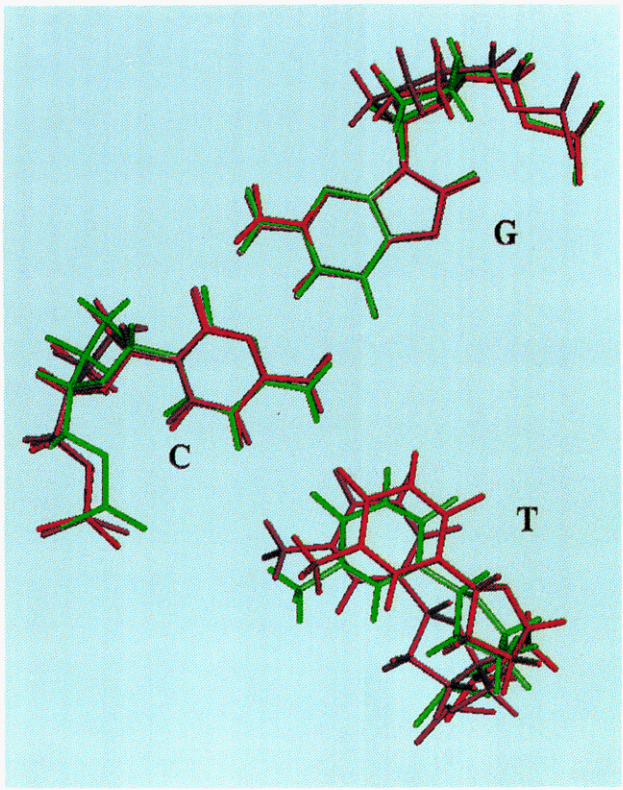

FIGURE 5: Relative mobility of the thymine base with respect to the Watson−Crick pair in the mismatch triplet plane.

average fluctuations. Again, the first and the last base triplet planes were not included in the calculation of the hydrogen bonds. Figure 4 presents the four hydrogen bonds between the bases in plane 4 and the distance between CN4·TH3 as a function of the simulation time. The first three panels give the hydrogen bond distances between the G_4·C_{11} Watson−Crick base pair, and the fourth panel presents the CN4·TO4 hydrogen bond. In the initial model structure, the distance between CN4 and TO4 was about 4.4 Å. Immediately after the equilibration of the solvent around the rigid triplex (after the first 60 ps of the trajectory) this distance was reduced to about 3.0 Å and fluctuated around an average of 2.88 ± 0.15 Å, indicating a stable hydrogen bond. In the fifth panel of Figure 4, we present another interatomic distance within the mismatch plane, namely, the distance between CN4 and TH3. The distance between these two atoms in the model-build structure was 3.2 Å, but after equilibration the distance fluctuated between 3.0 and 5.0 Å. This indicates a high degree of motion of the thymine base, which may contribute favorably to the entropy of binding. Bond distances given in Figure 2 indicate that the hydrogen bonds between Watson−Crick base pairs are stable and the C_{11} and T_{18} bases display a stable hydrogen bond between CN4 and TO4, even though the model-build structure did not.

Figure 5 presents a color-coded picture of the largest, average, and smallest fluctuation of the mismatch triplet, G_8C_{11}·T_{18}. To illustrate the relative mobility of the thymine base in the mismatch triplet plane, the Watson−Crick base pairs corresponding to the lowest and the highest rms deviations were least-squares fitted to that of the mean. (Note: only the heavy atoms in guanine and cytosine bases were used in the fitting procedure.) It is apparent that while the cytosine and guanine bases have maintained their Watson−Crick base pairing with the three hydrogen bonds between them, the thymine base possesses large in-plane relative mobility, maintaining the one possible hydrogen bond between the cytosine base and itself. It is interesting to see that the O4 of thymine was always directed toward the N4 of cytosine to form the hydrogen bond while the rest of the nucleoside displays an in-plane movement. This large in-plane motion of the thymine base is correlated with the sugar pucker and the motion of the phosphate backbone connected to the thymine base as well as the local helical parameters, especially the twist angle. The present simulation study shows that, even though the Watson−Crick pair does not show a large deviation from its in-plane alignment, the thymine base undergoes about a 20° deviation from a planar alignment relative to its average position. With these large fluctuations of the thymine base, the overall triplex is still stable over the 1.5 ns long trajectory. The role of the solvent in stabilizing the triplex will be discussed later.

Pseudorotation of the furanose rings was calculated as a function of the simulation time and is presented in Figure 6. The three columns and five rows of Figure 5 represent the three strands and five central base planes (from plane 2 to plane 6) of the triplex, respectively. The top two rows show a higher mobility for the bases while the bottom two rows indicate a relatively lower mobility of the triplex, consistent with the helical parameters given in Table 3. The middle row gives the sugar pucker of the mismatch triplet. The conformational change of pseudorotations of T_{18} and G_{17} at 1300 ps was correlated with the changes seen in the helical parameters. The second strand basically retains the A-form structure and displays low mobility, although more than for the homopolymer (Weerasinghe et al., 1995). Pseudorotation of the furanose rings of the 3′ end of the first strand displays transitions between C3′-*endo* and C2′-*endo* configurations, indicating B-form character. On the other hand, the 5′ end of the first strand adopts an equilibrium containing the C3′-*endo* configuration preferring an A-form DNA. Recent

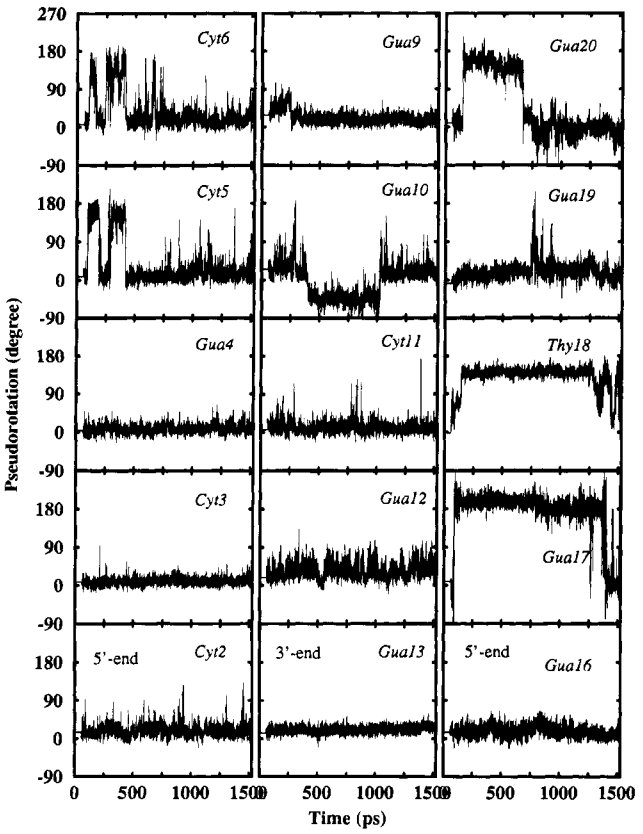

FIGURE 6: Pseudorotation of the furanose rings as a function of the simulation time.

NMR conformational studies by Dittrich et al. reported that the flanking CG•G base triplets are well-defined on the 5′ side of the thymine base while the base triplets on the 3′ side of thymine are somewhat disrupted (Dittrich et al., 1994). Even though the pseudorotation of the third strand does not show this difference clearly, the 3′ end of the third strand displays more flexibility than the 5′ end of the triplex. It has been found, with different potential force fields, that the internal energy of B-form nucleotides as a function of the pseudorotation angle features a double-well potential profile with a relatively small energy barrier, while that for A-form nucleotides gives a single-well potential profile (V. Pechenaya, W. R. Rudnicki, T. Grycuk, and B. Lesyng, unpublished results). This finding indicates that the 3′ end of the triplex with respect to the third strand displays an equilibrium shifted toward B-like configurations with the other parts of the triplex displaying an equilibrium closer to an A-like structure. The overall pattern of the conformational equilibria may be compared with the previous control simulation $(CG•G)_7$ (Weerasinghe et al., 1995). In that system the interconversion between cytosine sugar puckers was found to be more facile than that of this system. The observed pucker mobility of the flanking guanines and that of the third strand in this study appears to be a consequence of the central mismatch.

The torsional angles of the phosphate backbone and their variations provide a useful measure of the structure and the stability of the triplex. Furthermore, the torsional angle, δ, strongly correlates with the sugar pucker conformation of the triplex. Average torsional angles (and fluctuations) of the phosphate backbone are given in Table 5. The average torsional angles of the phosphate backbone of the first and the second strands show basically A-like conformations and remain close to their initial values with small fluctuations. The smaller standard deviations of the δ dihedral of the first and the second strands indicate less mobile structures with A-DNA-like conformations. The dihedral angles of G_{10} show relatively larger deviations. As given in Figure 6, pseudorotation of furanose in the G_{10} base shows C3′-*endo* to C2′-*endo* transitions and is consistent with the deviation of other dihedral angles in G_{10}. The average torsional angles of the third strand show a higher mobility and have an equilibrium with both A- and B-like conformations. Average dihedrals of strands I and II are generally in agreement with the X-ray fiber diffraction data (Piriou et al., 1994), while the third strand ϵ and ξ dihedrals show deviations from the starting structure.

(B) Solution Structure and Energetics. The distribution of the solvent molecules and counterions around DNA and the composition of the overall solution environment (Griffin & Dervan, 1989) influence the structure of the DNA. In addition, the equilibrium structure and diffusional properties

Table 5: Average Dihedral Angles (and Fluctuations) of the Phosphate Backbone in the Triplex

residue	α $n^a = 2$	β $n = 0$	γ $n = 3$	δ $n = 2$	ϵ $n = 0$	ξ $n = 2$	χ $n = 3$
initial dihedral	−66	168	55	88	−155	−69	−138/−152
C_2	−84(12)	165(13)	53(11)	80(07)	−155(09)	−68(08)	−150(10)
C_3	−73(09)	170(08)	58(09)	78(06)	−160(07)	−70(07)	−156(09)
G_4	−68(08)	179(09)	65(09)	83(06)	−143(11)	−66(08)	−165(08)
C_5	−70(09)	174(10)	58(09)	83(08)	−156(09)	−72(08)	−156(13)
C_6	−70(09)	176(09)	59(09)	82(09)	−155(10)	−74(10)	−146(14)
initial dihedral	−70	172	62	87	−153	−67	−145/−154
G_9	−75(09)	176(11)	57(10)	78(06)	−144(17)	−64(08)	−169(08)
G_{10}	−86(22)	132(41)	114(45)	94(17)	−141(19)	−70(09)	−180(06)
C_{11}	−69(09)	169(10)	57(09)	86(06)	−150(09)	−64(07)	−157(09)
G_{12}	−71(08)	176(08)	64(08)	81(07)	−152(09)	−68(08)	−166(07)
G_{13}	−76(09)	178(08)	46(09)	72(06)	−151(07)	−70(07)	−163(07)
initial dihedral	−124	124	61	72	59	72	−161/−135
G_{16}	−102(33)	154(19)	53(12)	76(07)	39(12)	79(11)	−147(10)
G_{17}	−106(11)	172(10)	55(09)	133(07)	−152(09)	−86(10)	−87(09)
T_{18}	−80(12)	160(12)	47(13)	122(14)	−108(29)	−173(22)	−75(15)
G_{19}	−73(10)	138(20)	51(14)	85(10)	−101(87)	−116(70)	−133(11)
G_{20}	−72(12)	146(24)	177(07)	97(22)	−114(44)	−137(45)	−96(18)

[a] n = the multiplicity of the intrinsic dihedral angle potential. $n = 2$ gives minima at 90° and −90° while $n = 3$ gives minima at 60°, −180°, and −60°.

Table 6: Locations and Magnitudes of the Extrema in the Pair Correlation Functions and Coordination Numbers for Water Pairs and Water-Ion Pairs

	first peak			
$g(r)$	height	maximum (Å)	minimum (Å)	coord no.
O−O	3.18	2.78	3.39	4.2
O−H	1.65	1.78	2.43	1.6
H−H	1.50	2.38	2.98	4.8
Na^+−O	9.87	2.38	3.13	5.2
Na^+−H	3.49	3.00	3.78	13.3
Cl^-−O	4.56	3.28	3.98	7.5
Cl^-−H	4.16	2.28	3.08	7.0
Na^+−N7	21.86	2.43	3.23	3.7
Na^+−OP	13.12	2.03	2.93	7.9

of the solvent and ions may be strongly influenced by the presence of a polyelectrolyte solute. The calculated characteristics of the radial pair distribution functions are summarized in Table 6. Average water−water correlations show little change from bulk at this concentration, in accord with the homopolymer study (Weerasinghe et al., 1995). In this study we find that the average number of water−oxygens around a Na^+ ion is 5.2 compared to 5.0 for the homopolymer and a value of 6.0 for an isolated sodium ion as reported by Impey et al. (1983). These results are in qualitative agreement with previously reported comparable studies (Weerasinghe et al., 1995; Smith et al., 1991; Forester & McDonald, 1991; van Gunsteren et al., 1986). The coordination number of Cl^- ions shows agreement with reported simulation results not containing DNA (Impey et al., 1983) as well as with our control study (Weerasinghe et al., 1995), suggesting that the Cl^- ions do not significantly interact with the triplex.

The average structural properties of the solvent and the counterions obtained from the traditional spherical radial distribution functions (Allen & Tildesley, 1987) do not reflect the effects of the presence of a macromolecular solute in the system in a manner which makes interpretation (assignment) simple (Brooks et al., 1988). Hence, to further study the solvation of DNA in the saline solution, cylindrical distribution functions of the solvent and the counterions with respect to the helical axis in the system were calculated (Forester & McDonald, 1991; Mohan et al., 1993b; Weerasinghe et al., 1995). The distribution functions for water and Na^+ around the triplex are given in panels a and b of Figure 7, respectively. The solid line gives the distribution of water (and Na^+ ions) obtained for a flexible solute, while the dashed line indicates the distribution found around rigid DNA obtained during the equilibration. Flexibility of the triplex appears to have an influence on how smooth the distribution of the solvent around the solute it, as has been seen previously (Weerasinghe et al., 1995; Mohan et al., 1993b). Averaging over a 1.4 ns long trajectory also provides better statistics for the distribution in the flexible case as opposed to the shorter rigid case.

The area under the small peak at 1.4 Å in the water distribution (Figure 7a) corresponds to one water molecule. That is, on average, one water molecule stays very close to the helical axis throughout the trajectory. However, exchange of the occupant of that position occurred. Two individual water molecules were found within a 2 Å distance from the helical axis with long residence time. Diffusion of those two water molecules from the helical axis is given in Figure 8a. The dashed line indicates the diffusion of the water molecule denoted by H_2O_1, and the solid line gives

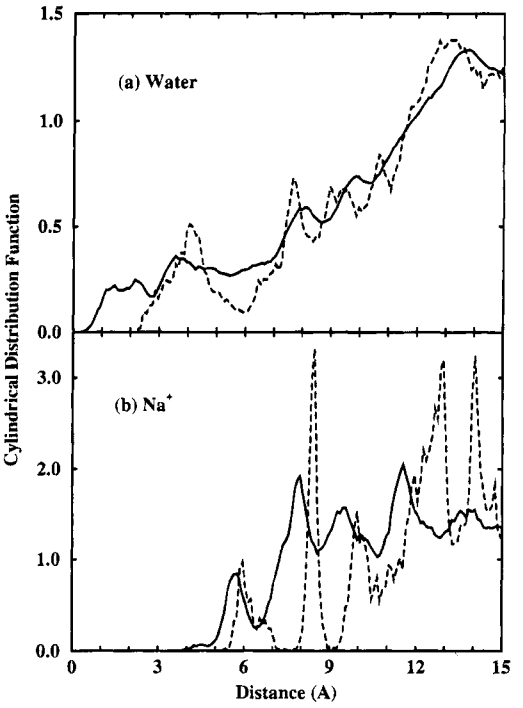

FIGURE 7: Cylindrical distribution of (a) water and (b) Na^+ ions around the triplex (solid line, flexible triplex; dashed line, rigid triplex).

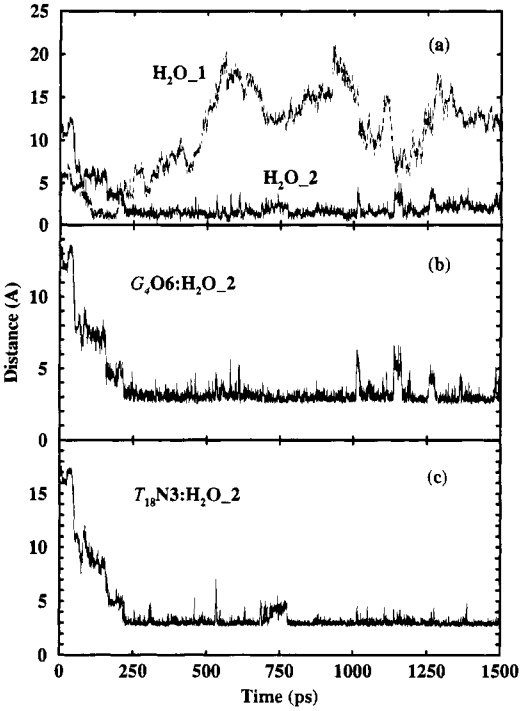

FIGURE 8: Plot of (a) the diffusion of H_2O_1 (dashed line) and H_2O_2 (solid line) from the helical axis, (b) the distance between G_4O_6 and H_2O_2, and (c) the distance between $T_{18}N3$ and H_2O_2 as a function of simulation time.

the diffusion of H_2O_2. It was found, by inspection, that the H_2O_1 molecule was positioned at the center of the GC•T mismatch triplet and, after about 200 ps, was exchanged by H_2O_2. Figure 8a indicates that the second water molecule remains bound to the mismatch triplet for the rest of the trajectory. Thus, a meaningful average residence time cannot be inferred from a simulation of this length. The hydrogen bonds between H_2O_2 with each of the G_4O6 and $T_{18}H3$

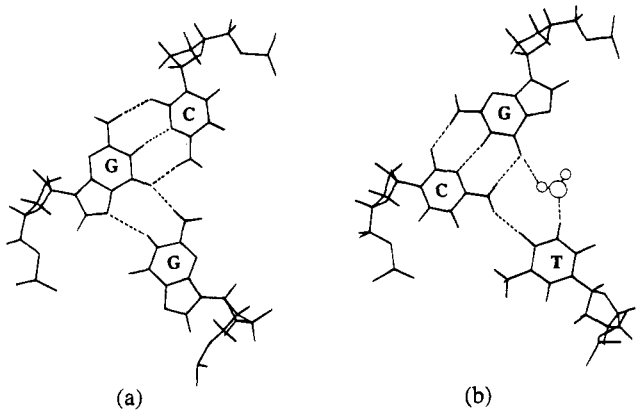

FIGURE 9: Sketch of hydrogen bonds (a) between the CG•G triplet and (b) between bases in the GC•T triplet along with the coordinated water molecule.

groups are presented in panels b and c of Figure 8, respectively. This clearly indicates that the water molecule is involved in forming bridging hydrogen bonds between G_4 and T_{18}. Complementary data for H_2O-1 also confirm this structural motif (not shown). Figure 9 gives a snapshot of the G_4C_{11}•T_{18} triplet, together with the coordinated water molecule and the C_3G_{12}•G_{17} triplet, after 800 ps of the trajectory (dashed lines are to indicate hydrogen bonds between bases). Figure 9 shows that there are two possible hydrogen bonds between G_4 and C_{11} bases, while there is only one possible hydrogen bond between C_{11} and T_{18} bases. These results indicate that there is a secondary structural element between G_4 and T_{18} mediated by a water molecule. This type of water-mediated hydrogen bond in biopolymers has been observed previously for nucleic acid systems (Mohan et al., 1993a; Subramaniam et al., 1988), for a protein–DNA system (de Vlieg et al., 1989), and in protein active sites (Brooks et al., 1988).

The peak in the water distribution beyond 3.0 Å (Figure 7a) is due to the spine of hydration associated with CG•G triple helices in the so-called M1 groove (Mohan et al., 1993a). This feature has been previously assigned, and the number of water molecules contributing to this spine is in accord with previous studies. The spine water at the mismatch is closer to the helix center, due to the different geometry of the GC•T plane and its own equilibrium helical parameters such as slide and shift. Solvation of triplex DNA in solution, which is believed to be a major factor in the stability of DNA triplexes, involves water molecules with long residence times. Recent NMR studies by Patel and co-workers reported on hydration structures in triplex systems (Radhakrishnan & Patel, 1994a,b). Recent work from this laboratory using computer simulations predicted the existence of a spine of hydration and salt structures in py•pu•pu anti-parallel systems (Mohan et al., 1993b). The NMR work found structures proximal to strands II and III in both pu•pu•py and py•pu•py DNA triplexes while the NMR assessment of hydration structures between strands I and III of py•pu•pu was difficult due to the ambiguities inherent in the interpretation of the data (Radhakrishnan & Patel, 1994a,b).

We now consider the details of the salt structures and their comparison with our previous results on homooligomer sequences. The solid line of Figure 7b gives the cylindrical distribution of Na^+ ions around the flexible triplex while the

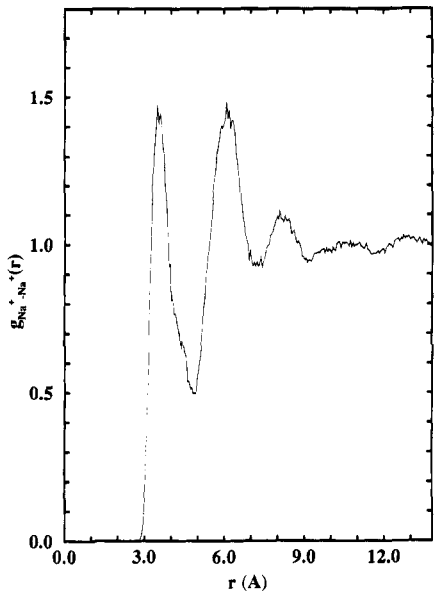

FIGURE 10: Sodium–sodium spherical radial distribution function.

dashed line presents the same for the rigid triplex. Again, the length of the trajectory and the flexibility of the triplex have an influence on the smoothness of the distribution. The area under the first and the second peaks corresponds to three Na^+ ions. It was found that, on average, one Na^+ ion was bound to the N7 atoms of both the G_{19} and G_{20} bases while another two ions were bound to the N7 atoms of the G_{16} and G_{17} bases. There were no Na^+ ions observed to be close to the mismatch base plane during the simulation. Integrating the cylindrical distribution function of Na^+ ions to 13 Å corresponds to nine Na^+ ions (the average distance to the P atom in a phosphate group from the helical axis is 10 Å), which is in a reasonable agreement with the coordination number of Na^+ ions around phosphate oxygens calculated from the radial distribution function (Table 6) and that observed for the control simulation (Weerasinghe et al., 1995).

The Na^+ ion pair distribution is given in Figure 10. The first peak near 3.5 Å indicates that there are a few Na^+ ion pairs in the system. The simulation displayed several, short-lived, Na^+ ion pairs, and in particular, one pair of ions was found next to the phosphate group of G_{13}. Both sodium ions were coordinated to the G_{13} phosphate group and stay in contact for about 100 ps. There were several pairs found coordinated to different phosphate groups, and they were short-lived. Interestingly, there was one pair of Na^+ ions found in solution, away from the solute, that remained "paired" for nearly 200 ps. Unstable local minima in the interionic potential of mean force for like ions have been the subject of theoretical (Pettitt & Rossky, 1986) and simulation (Dang et al., 1992) studies. On average, both ions maintained six coordinated water molecules around them during this time period; two water molecules were shared by both ions and formed a close square-planar structure. There were four other water molecules around each ion to complete their first hydration shells. The intensity of the first peak is less than that for the corresponding homooligomer (Weerasinghe et al., 1995), indicating less ion pairing with the mismatch. Irregularity of the structure and hence the electrostatic field may play a role in breaking up such ion pairings. The second broad peak of the distribution at

6.5 Å indicates that there are Na^+ ion pairs which interact with each other via their first hydration shell. This feature has been observed previously for MD simulations of nucleic acid systems in salt solutions (Weerasinghe et al., 1995; Mohan et al., 1993b; Forester & McDonald, 1991).

Diffusion coefficients of water, Na^+, and Cl^- ions were also calculated in order to examine the influence on the mobility of the solvent and ions around the triplex DNA. A simple proximity classification was used to consider the spatial dependence of diffusion in the system. All the water molecules and Na^+ ions remaining within 3.5 Å of any atom of the triplex DNA were classified as bound species, and the rest were considered as unbound. With this classification, three different values were calculated for the water and Na^+ ions, namely, average, bound, and unbound diffusion coefficients. The average diffusion coefficients of water and Na^+ and Cl^- ions are 1.4×10^{-9}, 0.4×10^{-9}, and 0.8×10^{-9} m^2 s^{-1}, respectively. These may be compared with the previous values around the homopolymer of 1.3×10^{-9}, 0.3×10^{-9}, and 0.9×10^{-9} m^2 s^{-1}, respectively. The average diffusion coefficients were lower than the results obtained from MD simulations of pure water and salt−water solutions (Berendsen et al., 1987; Smith & Pettitt, 1991; Berkowitz & Wan, 1987). Diffusion coefficients of bound Na^+ ions and water molecules were 0.2×10^{-9} and 0.8×10^{-9} m^2 s^{-1}, respectively, with unbound values of 0.6×10^{-9} and 1.6×10^{-9} m^2 s^{-1} for sodium and water. Even though the diffusion coefficients of unbound species are higher than the average coefficients, they are lower than the diffusion coefficients of the same entities in salt solution without a biomolecular solute (33% lower for water and 50% lower for Na^+). As both water and sodium diffusion is reduced, electrostatic and excluded volume effects must be significant. It is interesting to note that the diffusion coefficients of water and ions from this work and from the simulation of a homopolymer triplex DNA (Weerasinghe et al., 1995) with the same force field are essentially in agreement, well within the statistical uncertainty of ± 0.1 m^2 s^{-1}, indicating that the presence of a mismatch in the triplex DNA does not have a great influence on the mobility of the solvent and ions in the solution even though the mismatch strongly affects the DNA dynamics and structure.

DISCUSSION

The simulation results show that, with respect to a model-built structure, the third strand with the mismatch has the largest rms deviation, while the second strand shows the smallest deviation from the model-built triplex DNA. The mismatched thymine base and the attached phosphate group show the largest rms deviations compared to the other bases and corresponding phosphate groups. Despite the higher mobility of the thymine base in the mismatch triplet, the overall rms deviation of the triplex is less than 2.0 Å over the 1.5 ns long trajectory. Our simulation results further indicate that there is a long-lived water-mediated secondary hydrogen bond between the G_4 and T_{18} bases. One water molecule was involved in bridging between the G_4 and T_{18} bases within the first 100 ps of the trajectory, and after about 200 ps, another water molecule came in and replaced the former. The second water molecule stayed at the middle of the mismatch triplet during the rest of the trajectory. The coordination of a water molecule, between the G_4 and T_{18} of the mismatch triplet, may be a contributing factor in the overall stability of the triplex, considering the large local motions of the thymine base. Coordination of water molecules between bases in the first and the third strands of triplex DNA has been reported earlier and is thought to help to stabilize the system energetically (Mohan et al., 1993a; Radhakrishnan & Patel, 1994a). These effects would be difficult to model by simpler solvation treatments (Cheng & Pettitt, 1992a, 1995). Overall rms deviations of the strands, bases, sugars, and phosphate groups in the homopolymer triplex (Weerasinghe et al., 1995) and the triplex with a GCT mismatch in this study appear to be the same within statistical uncertainty. This indicates that even though the thymine base, and the phosphate group next to it, has higher mobility, other parts of the triplex compensate with lower rms deviations.

Dittrich et al. (1994) have reported that the refined NMR structure of the GC·T triplet shows a possible hydrogen bond between CN4·TO4 and a distortion of the in-plane alignment of the three bases. More recently, Gao and co-workers (Ji and Gao, unpublished results) have performed a complementary high-resolution structure analysis by NMR which strongly confirms the presence of this hydrogen bond. Our simulation developed a stable hydrogen bond between C_{11} and T_{18}. The system maintained a planar alignment between the Watson−Crick base pair in the mismatch triplet and displayed about a 20° deviation from the initial in-plane alignment between G_4 and T_{18} base planes, which is consistent with the above NMR findings. The hydrophobic nature of the methyl group of the thymine base may be the reason for the deviation from the initial in-plane alignment of the mismatch triplet plane.

Penetration of solvent molecules and ions into the grooves was more visible with the flexible triplex DNA than with the rigid structure, consistent with MD simulation studies of triplex DNA in salt−water solutions (Weerasinghe et al., 1995). Several Na^+ ions were found to be bound simultaneously to both the N7 of guanine bases in strand III and nearby phosphate groups. Interestingly, there were no sodium ions found lying along the bisector of the O−P−O angle of a phosphate group. On average, there were 19 Na^+ ions within 4.0 Å from P atoms in the backbone of the triplex. Counterion condensation (*or* Manning) theory (Manning, 1991) predicts a total of 18 condensed Na^+ ions and is in a good agreement with the simulation results.

CONCLUSION

The results obtained from a simulation of a reverse-Hoogsteen antiparallel model DNA triple helix, with a GC·T mismatch at the middle of the triplex, in 1 M saline solution support recent NMR experimental conclusions for the same mismatch triplex system. In addition, they suggest that coordination of a water molecule between G_4 and T_{18} is a plausible structural feature and may explain the presence of both hydrogen-bonded and non-hydrogen-bonded GT pairs found in the NMR study (Dittrich et al., 1994). The importance of such structural waters for the thermodynamic stability of triplexes was previously postulated (Mohan et al., 1993a), and the existence of a spine of hydration has since been inferred from FTIR measurements (White & Powell, 1995).

The internal consistency of the simulation was reflected in the overall rms deviation (1.8 Å), a reasonable value

despite higher fluctuations observed in the thymine base and attached phosphate group. The three strands remained intact during the 1.5 ns long trajectory, even though the model triplex is less than a full helical turn, lending credibility to the model triplex. It is interesting to note that regions of the triplex above and below the mismatch displayed a higher and lower helical rise and twist, and yet the overall rms deviation still remains low. Sugar pucker and backbone dihedral angles indicate that strand II possesses an A-like conformation while strands I and III display an equilibrium between A, B, and other forms. Deviations from the initial model-built structure are largest for the backbone dihedral angles of strand III, which is reflected in a higher mobility.

Complete equilibration of ions, solvent, and the triplex appeared to be achieved within the first 700−800 ps of the trajectory. Diffusion coefficients of ions and water are consistent, within statistical uncertainty, to the results for a homopolymer $(CG{\cdot}G)_7$ DNA triplex (Weerasinghe et al., 1995), indicating that the presence of a mismatch triplet in the present study does not have an effect on the bulk mobility of ions and water around the triplex. Coordination of a water molecule between G_4 and T_{18} appears to play a role in the stability of the triplex. Whether it is possible to detect such a water molecule by NMR spectroscopy depends on whether the time scale for exchange is sufficiently long, something not reliably ascertained from this study. It is apparent, however, that water-mediated hydrogen-bonding effects will have to be taken into consideration when trying to understand or predict the interaction between the bases contained in the third strand and those within the duplex DNA.

REFERENCES

Allen, M. P., & Tildesley, D. J. (1987) *Computer Simulation of Liquids*, 1st ed., Oxford University, New York.

Beal, P. A., & Dervan, P. B. (1992) *Nucleic Acids Res. 20*, 2773−2776.

Berendsen, H. J. C., Grigera, J. R., & Straatsma, T. P. (1987) *J. Phys. Chem. 91*, 6269−6274.

Berkowitz, M., & Wan, W. (1987) *J. Chem. Phys. 86*, 376−382.

Brooks, B. R., Bruccoleri, R. E., Olafson, B. D., States, D. J., Swaminathan, S., & Karplus, M. (1983) *J. Comput. Chem. 4*, 187−198.

Brooks, C. L., III, Karplus, M., & Pettitt, B. M. (1988) in *Advances in Chemical Physics* (Prigogine, I., & Rice, S. A., Eds.) Vol. 71, John Wiley & Sons, New York.

Chandrasekhar, J., Spellmeyer, D. C., & Jorgensen, W. L. (1984) *J. Am. Chem. Soc. 106*, 903−910.

Cheng, Y., & Pettitt, B. M. (1992a) *J. Am. Chem. Soc. 114*, 4465−4474.

Cheng, Y., & Pettitt, B. M. (1992b) *Prog. Biophys. Mol. Biol. 58*, 225−257.

Cheng, Y., & Pettitt, B. M. (1995) *Biopolymers 35*, 457−473.

Dang, L. X., Pettitt, B. M., & Rossky, P. J. (1992) *J. Chem. Phys. 96*, 4046−4047.

de Leeuw, S. W., Perram, J. W., & Smith, E. R. (1980) *Proc. R. Soc. London 373A*, 27−39.

de Vlieg, J., Berendsen, H. J. C., & van Gunsteren, W. F. (1989) *Proteins 6*, 104−127.

Dittrich, K., Gu, J., Tinder, R., Hogan, M., & Gao, X. (1994) *Biochemistry 33*, 4111−4120.

Ewald, P. (1921) *Ann. Phys. 64*, 253−264.

Forester, T. R., & McDonald, I. R. (1991) *Mol. Phys. 72*, 643−660.

Greenberg, W. A., & Dervan, P. B. (1995) *J. Am. Chem. Soc. 117*, 5016−5022.

Griffin, L. C., & Dervan, P. B. (1989) *Science 245*, 967−971.

Hélène, C., & Toulme, J. J. (1990) *Biochim. Biophys. Acta 1049*, 99−125.

Impey, R. W., Madden, P. A., & McDonald, I. R. (1983) *J. Phys. Chem. 87*, 5071−5083.

Kim, S. H., Suddath, F. L., Quigley, G. J., McPharson, A., Sussman, J. L., Wang, A. J. H., Seeman, N. C., & Rich, A. (1974) *Science 185*, 435−440.

Laughton, C. A., & Neidle, S. (1992) *J. Mol. Biol. 223*, 519−529.

Letai, A. G., Palladino, M. A., Fromm, E., Rizzo, V., & Fresco, J. R. (1988) *Biochemistry 27*, 9108−9112.

Manning, G. S. (1991) in *Theoretical Biochemistry & Molecular Biophysics: DNA* (Beveridge, D. L., & Lavery, R., Eds.) Vol. 1, Adenine Press, New York.

McCammon, J. A., & Harvey, S. C. (1987) *Dynamics of Proteins and Nucleic Acids*, 1st ed., Cambridge University Press, Cambridge.

Mergny, J. L., Sun, J. S., Rougée, M., Montenary-Garestier, T., Barcelo, F., Chomillier, J., & Hélène, C. (1991) *Biochemistry 30*, 9791−9798.

Mohan, V., Smith, P. E., & Pettitt, B. M. (1993a) *J. Am. Chem. Soc. 115*, 9297−9298.

Mohan, V., Smith, P. E., & Pettitt, B. M. (1993b) *J. Phys. Chem. 97*, 12984−12990.

Ouali, M., Letellier, R., Sun, J.-S., Akhebat, A., Adent, F., Liquier, J., & Taillandier, E. (1993) *J. Am. Chem. Soc. 115*, 4264−4270.

Pettitt, B. M., & Rossky, P. J. (1986) *J. Chem. Phys. 84*, 5836−5844.

Piriou, J. M., Ketterlé, J. Ch., Gabarro-Arpa, J., Cognet, J. A. H., & Le Bert, M. (1994) *Biophys. Chem. 50*, 323−343.

Radhakrishnan, I., & Patel, D. J. (1993) *Structure 1*, 135−152.

Radhakrishnan, I., & Patel, D. J. (1994a) *Biochemistry 33*, 11405−11416.

Radhakrishnan, I., & Patel, D. J. (1994b) *Structure 2*, 395−405.

Robertus, J. D., Ladner, J. E., Finch, J. T., Rhodes, D., Brown, R. S., Clark, B. F. C., & Klug, A. (1974) *Nature 250*, 546−551.

Ryckaert, J. P., Ciccotti, G., & Berendsen, H. J. C. (1977) *J. Comput. Phys. 23*, 327−349.

Singleton, S. F., & Dervan, P. B. (1994) *J. Am. Chem. Soc. 116*, 10376−10382.

Smith, P. E., & Pettitt, B. M. (1991) *J. Am. Chem. Soc. 113*, 6029−6037.

Subramaniam, P. S., Ravishanker, G., & Beveridge, D. L. (1988) *Proc. Natl. Acad. Sci. U.S.A. 85*, 1836−1840.

Sun, J. S., & Hélène, C. (1993) *Curr. Opin. Struct. Biol. 3*, 345−356.

Swaminathan, S., Ravishanker, G., & Beveridge, D. L. (1991) *J. Am. Chem. Soc. 113*, 5027−5040.

Swope, W. C., Andersen, H. C., Berens, P. H., & Wilson, K. R. (1982) *J. Chem. Phys. 76*, 637−649.

Vlijmen, H. W. T. V., Ramé, G. L., & Pettitt, B. M. (1990) *Biopolymers 30*, 517−532.

Weerasinghe, S., Smith, P. E., Mohan, V., Cheng, Y., & Pettitt, B. M. (1995) *J. Am. Chem. Soc. 117*, 2147−2158.

White, A. P., & Powell, J. W. (1995) *Biochemistry 34*, 1137−1142.

Wilson, W. D., Tanious, F. A., Mizan, S., Yao, S., Kiselyov, A. S., Zon, G., & Strekowski, L. (1993) *Biochemistry 32*, 10614−10621.

BI951620T